Redescription of the Cranium of *Jingshanosaurus xinwaensis* (Dinosauria: Sauropodomorpha) from the Lower Jurassic Lufeng Formation of Yunnan Province, China

QIAN-NAN ZHANG,[1,2,3] TAO WANG,[4] ZHI-WEN YANG,[4] AND HAI-LU YOU[1,2,3]*

[1]Key Laboratory of Vertebrate Evolution and Human Origins, Institute of Vertebrate Paleontology and Paleoanthropology, Chinese Academy of Sciences, 142 Xizhimenwai Street, Beijing, 100044, China

[2]CAS Center for Excellence in Life and Paleoenvironment, 142 Xizhimenwai Street, Beijing, 100044, China

[3]College of Earth and Planetary Sciences, University of Chinese Academy of Sciences, 19A Yüquan Road, Beijing, 100049, China

[4]Bureau of Land and Resources of Lufeng County, Yunnan Province, 651299, China

ABSTRACT

The Lower Jurassic Lufeng Formation in Yunnan Province of southwestern China has yielded an important and diverse terrestrial vertebrate fauna dominated by basal sauropodomorph dinosaurs. Nevertheless, many of them lack detailed descriptions and/or explicit diagnoses, hampering systematic analyses of their interrelationships and further studies. We present a detailed redescription of the cranial osteology of *Jingshanosaurus xinwaensis* and amend its diagnosis. Incorporation of the revised anatomical data into a phylogenetic analysis finds *Jingshanosaurus* to be one of the earliest diverging sauropodiforms. Moreover, the previously reported *Chuxiongosaurus lufengensis* is considered to be a junior synonym of *J. xinwaensis*. *Jingshanosaurus* can be diagnosed by a unique combination of character states, including (1) an inflection at the base of the dorsal premaxillary process; (2) the level of the caudal margin of the external naris being caudal to the mid-length of the maxillary tooth row and the rostral margin of the antorbital fenestra; (3) a ventrally constricted subtriangular orbit; (4) the height-to-length ratio of the dentary being greater than 0.2; and (5) a distally recurved long axis of the premaxillary and rostral maxillary tooth crowns. As the largest taxon (around 9 m long) currently known among Lufeng basal sauropodomorphs and one of the best known basal-most sauropodiforms, a better understanding of *Jingshanosaurus* will allow for reconstruction of the ecomorphotypic diversity of the Lower Jurassic Lufeng dinosaurs and help to decipher the origin and early evolution of sauropodiforms, the clade ultimately leading to the gigantic sauropods. Anat Rec, 00:000–000, 2019. © 2019 Wiley Periodicals, Inc.

Additional Supporting Information may be found in the online version of this article.

Grant sponsor: National Natural Science Foundation of China; Grant numbers: 41472020, 41688103, 41872021; Grant sponsor: The Strategic Priority Research Program of Chinese Academy of Sciences; Grant number: XDB26000000; Grant sponsor: Chinese Academy of Sciences.

*Correspondence to: Hai-Lu You, Institute of Vertebrate Paleontology and Paleoanthropology, Chinese Academy of Sciences, 142 Xizhimenwai Street, Beijing 100044, China.
E-mail: youhailu@ivpp.ac.cn

Received 12 July 2018; Revised 2 December 2018; Accepted 25 December 2018.

DOI: 10.1002/ar.24113

Published online 00 Month 2019 in Wiley Online Library (wileyonlinelibrary.com).

Key words: *Jingshanosaurus*; sauropodomorph; dinosaur; lower Jurassic; Lufeng formation

The Lower Jurassic Lufeng Formation of Yunnan Province in southwestern China has yielded an important and diverse terrestrial vertebrate fauna referred to as the "Lufeng Saurischian Fauna" (Young 1951), and within this formation, sauropodomorph dinosaurs are the dominant large herbivores. Since *Lufengosaurus huenei* was reported (Young 1941a), numerous sauropodomorph specimens have been recovered from the Lower Jurassic of Lufeng County (Young 1941b, 1942, 1947, 1951; Zhang and Yang 1995; Lü et al. 2010; Sekiya 2010; Sekiya and Dong 2010; Wang et al. 2017; Zhang et al. 2018). Although controversies still surround the species validity and precise interrelationships of some Lufeng taxa (e.g., "*Gyposaurus*" *sinensis*, *Lufengosaurus magnus*, and *Yunnanosaurus robustus*), the type species of *Lufengosaurus*, *Yunnanosaurus*, and *Jingshanosaurus* have been regarded as distinct taxa in taxonomic and systematic analyses (Galton and Cluver 1976; Cooper 1981; Galton 1990; Sereno 1999; Galton and Upchurch 2004; Barrett et al. 2005; Barrett et al. 2007; Smith and Pol 2007; Upchurch et al. 2007; Martínez 2009; Apaldetti et al. 2011; Apaldetti et al. 2013; Otero and Pol 2013; McPhee et al. 2015; McPhee and Choiniere 2017).

Based on an almost complete specimen (LFGT-ZLJ0113), *Jingshanosaurus xinwaensis* was erected as a member of Plateosauridae, which was supported by a general description of the material (Zhang and Yang 1995). Its phylogenetic position has been somewhat contentious since its discovery. For example, Upchurch et al. (2007) regarded this genus as more derived than *Lufengosaurus*, *Yunnanosaurus*, and *Anchisaurus*, and less derived than *Melanorosaurus* and other derived forms, whereas Yates (2007), Ezcurra (2010), Apaldetti et al. (2011), and Otero and Pol (2013) all suggested it to be more derived than *Lufengosaurus* but less derived than *Yunnanosaurus*, *Anchisaurus*, *Melanorosaurus*, and other derived sauropodomorph forms. Recently Wang et al. (2017) and McPhee and Choiniere (2017) recovered it as more derived than *Yunnanosaurus* but less derived than *Anchisaurus*, *Melanorosaurus*, and other derived forms, while Chapelle and Choiniere (2018) regarded it as less derived than *Lufengosaurus* and *Yunnanosaurus*. Part of the instability of *Jingshanosaurus*' phylogenetic position stems from the scoring of the cranial features of LFGT-ZLJ0113, which has depended on the original publication. Unfortunately, the original publication had unclear photographs and diagnoses. Based on further preparation, we present a detailed redescription on the cranium of the holotype, revise its morphological diagnoses, and analyze its phylogenetic position within Sauropodomorpha. Furthermore, Wang (2004) reported additional cranial material (CXM-LT9401) identified as *Jingshanosaurus* cf. *xinwaensis*. This same specimen was subsequently regarded as a new genus and species named *Chuxiongosaurus lufengensis* (Lü et al. 2010). Our re-examination shows that the anatomical features of CXM-LT9401 generally resemble those of LFGT-ZLJ0113, and our cladistic analysis suggests these two specimens form a sister group. Therefore, we regard *C. lufengensis* as a junior synonym of *J. xinwaensis* and refer CXM-LT9401 to *J. xinwaensis*.

Anatomical Abbreviations

an, angular; ar, articular; bo, basioccipital; bpt, basipterygoid process; bs, basisphenoid; d, dentary; ecp, ectopterygoid; exo, exoccipital-opisthotic; f, frontal; ic, intercoronoid; j, jugal; l, lacrimal; m, maxilla; n, nasal; p, parietal; par, prearticular; pl, palatine; pm, premaxilla; po, postorbital; pop, paroccipital process; pf, prefrontal; ps, parasphenoid; pt, pterygoid; q, quadrate; qj, quadratojugal; s, squamosal; sa, surangular; so, supraoccipital; sp, splenial.

Institutional Abbreviations

CXM, Chuxiong Prefectural Museum, Chuxiong, China; LFGT, Bureau of Land and Resources of Lufeng County, Lufeng, China.

MATERIALS AND METHODS

The holotype (LFGT-ZLJ0113) of *J. xinwaensis* was discovered by Mr. Zheng-Ju Wang of Cultural Affairs Station of Lufeng County in October, 1988 from the Shawan Member (Dull Purplish Beds) of Lufeng Formation at Xinwa Village, Town of Jinshan (Fig. 1). The fossil quarry is now located in the Lufeng Dinosaur National Geopark, which was erected because a number of dinosaur skeletons were discovered there. The holotype is nearly complete except for cervicals (C4-C10) and is now mounted for exhibition in the museum of Lufeng World Dinosaur Valley in Yunnan Province, China (see Supporting Information Fig. S1-A).

Most widely accepted data matrices that have included *J. xinwaensis* have based the cranial characters of *Jingshanosaurus* on the reconstructed, idealized cranium sketch presented by Zhang and Yang (1995). In light of the current redescription of the further prepared cranium, we investigate the potential effects of our revised character data on the phylogenetic positions of LFGT-ZLJ0113 and CXM-LT9401 based on the data matrices of McPhee and Choiniere (2017), and also add *Yizhousaurus* erected by Zhang et al. (2018). We have modified and supplemented the scoring of the cranial character states of these two specimens based on a combination of previous publications (Zhang and Yang 1995; Lü et al. 2010) and personal observations. One hundred and two out of the total 120 cranial characters used by McPhee and Choiniere (2017) had been previously scored for LFGT-ZLJ0113. Twenty-seven states have now been revised, of which 15 have been scored as "?". In addition, four new characters have been coded. Therefore, we are able to score a total of 91 characters for LFGT-ZLJ0113 (see Supporting Information Tables S3 and S4). Besides, we have coded 103 characters for CXM-9401 in this research (see Supporting Information Table S5).

The current data matrix is comprised of 364 characters and 61 taxa. Phylogenetic analyses were performed using

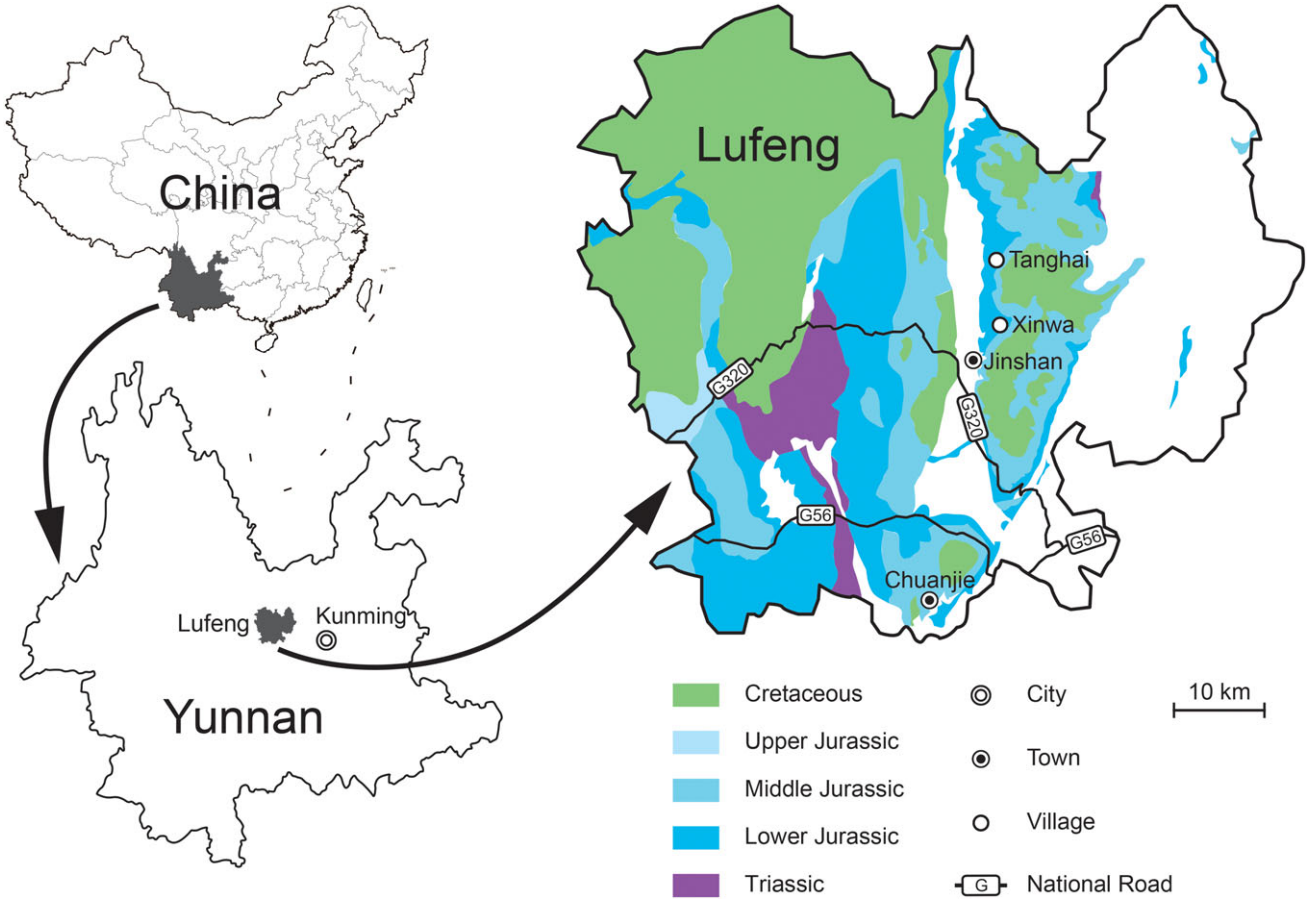

Fig. 1. Geographic position and stratigraphic distribution of taxa from the Lufeng Formation. LFGT-ZLJ0113 and CXM-LT9401 were recovered at Xinwa and Tanghai, respectively.

TNT (ver. 1.1), applying a heuristic search of 1,000 replicates of Wagner trees and tree bisection-reconnection (TBR) with 10 trees saved per replication. All characters were equally weighted, and 43 multistate characters were coded as ordered.

RESULTS

Systematic Paleontology

DINOSAURIA (Owen 1842).
SAURISCHIA (Seeley 1887).
SAUROPODOMORPHA (von Huene 1932).
MASSOPODA (Yates 2007).
SAUROPODIFORMES (Sereno 2007) (sensu McPhee et al. 2014).
JINGSHANOSAURUS (Zhang and Yang 1995).

Type species. *Jingshanosaurus xinwaensis* Zhang and Yang 1995.

Emended diagnosis. As for type species.
JINGSHANOSAURUS XINWAENSIS (Zhang and Yang 1995).
Jingshanosaurus cf. *xinwaensis* (Wang 2004).
Chuxiongosaurus lufengensis (Lü et al. 2010)

Holotype. LFGT-ZLJ0113 (field number: LV003), a well-preserved skeleton (around 9 m in total length) consisting of the skull with mandibles (Figs. 2–7), in articulation with the atlas-axis complex and the third cervical, 14 dorsals, 3 sacra, 38 caudals, and a nearly complete appendicular skeleton.

Referred specimen. CXM-LT9401, a well-preserved skull with mandibles.

Horizon and locality. Both specimens were recovered from the Shawan Member (Dull Purplish Beds) of the Lower Jurassic Lufeng Formation. LFGT-ZLJ0113 is from Xinwa Village, and CXM-LT9401 is from Tanghai Village of Town of Jinshan, Lufeng County, Yunnan Province, China.

Emended diagnosis. *(Cranial features only).* As a basal sauropodiform, *J. xinwaensis* can be diagnosed by a unique combination of character states (*represents autapomorphies present in LFGT-ZLJ0113 and/or CXM-LT9401): (1) inflection at the base of the dorsal premaxillary process (CXM-LT9401, also present in *Melanorosaurus*); (2) level of the caudal margin of the external naris caudal to the mid-length of the maxillary tooth row and the rostral

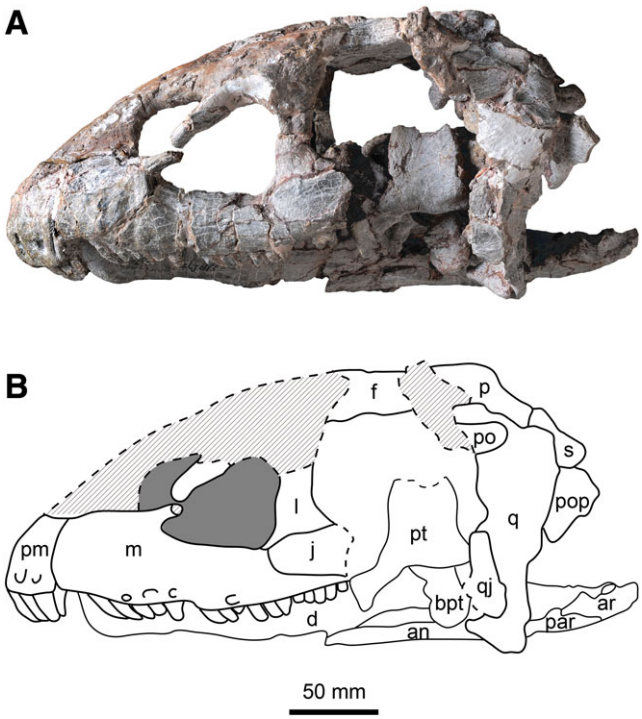

Fig. 2. Photograph **(A)** and interpretative line drawing **(B)** of the cranium of LFGT-ZLJ0113 in left lateral view. Dark gray fills represent openings, diagonal lines represent missing parts, and dashed lines represent fracture.

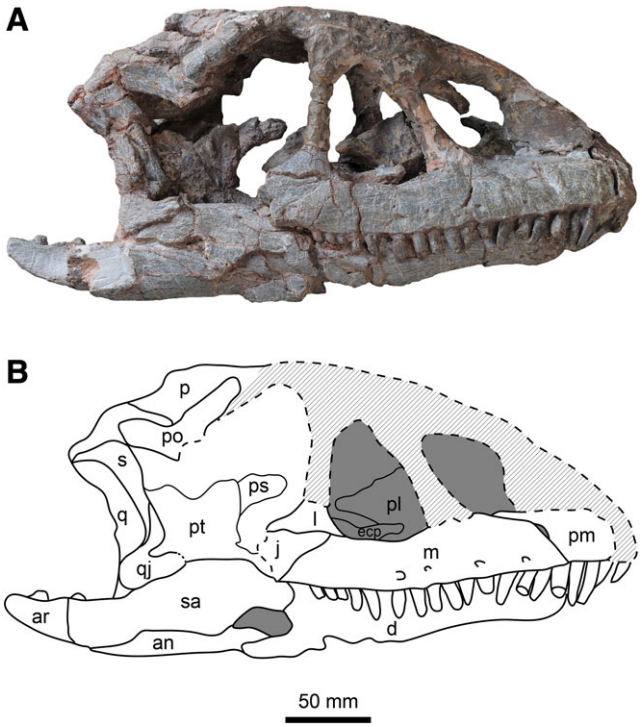

Fig. 3. Photograph **(A)** and interpretative line drawing **(B)** of the cranium of LFGT-ZLJ0113 in right lateral view. Dark gray fills represent openings, diagonal lines represent missing parts, and dashed lines represent fracture.

margin of the antorbital fenestra* (both LFGT-ZLJ0113 and CXM-LT9401); (3) slightly rostrodorsally sloping orientation of the lacrimal orbital margin; (4) ventrally constricted subtriangular orbit* (both LFGT-ZLJ0113 and CXM-LT9401); (5) rostrocaudally shortened jugal plate at suborbital region* (CXM-LT9401); (6) shape of the floor of the braincase in lateral view bent with the basal tubera below the level of the basioccipital and the parasphenoid rostrum raised above it (also present in *Melanorosaurus* and *Yizhousaurus*); (7) height-to-length ratio of the dentary greater than 0.2* (both LFGT-ZLJ0113 and CXM-LT9401); (8) length of the retroarticular process greater than the depth of the mandible below the glenoid (also present in *Coloradisaurus* and *Lufengosaurus*); (9) distally recurved long axis of the tooth crowns (both LFGT-ZLJ0113 and CXM-LT9401)*.

Comments. Zhang and Yang (1995) listed a large number of cranial characters in the original diagnosis of *J. xinwaensis*: skull small and elongated, equivalent in length to 2.4 times of the fourth cervical vertebrae or three times of the first caudal; cranial openings large, and bars separating the openings gracile; external naris large and subcircular; antorbital fenestra medium size and triangular; orbit large and subcircular; infratemporal fenestra dorsoventrally tall and trapezoidal; supratemporal fenestra small and circular; occipital region narrow, and occipital plate slightly sloped; skull roof flat; jaws slender, especially the mandibular rami; jaw articulation below the level of dentary tooth row; tooth row elongate, and teeth closely aligned; four premaxillary teeth elongate and robust, tooth crowns pointed and subcircular in cross-section; anterior maxillary teeth similar to premaxillary, and tooth crowns of mid-posterior ones oblate with weak serrations on both margins; dentary teeth elongate and robust, slightly oblate with distinct serrations. However, none of these features differ substantially from those seen in other basal sauropodomorphs (e.g., shape and size of cranial openings, tooth morphology and counts) and cannot be regarded as diagnostic for *Jingshanosaurus* (see later for further details). One feature noticed by the original authors, the distally recurved long axis of the premaxillary and anterior maxillary tooth crowns was regarded as one of the main differences between *Jingshanosaurus* and *Lufengosaurus* (Barrett et al. 2005).

Wang (2004) reported the cranial material (CXM-LT9401) and identified it as *Jingshanosaurus* cf. *xinwaensis.* This specimen was subsequently named as a new species, *C. lufengensis* by Lü et al. (2010) without mentioning aforesaid paper and regarded it as the most basal sauropod (equivalent to the most basal sauropodiform in McPhee and Choiniere's phylogeny). Lü et al. (2010) proposed four diagnoses for *C. lufengensis*: lacrimal perpendicular to the ventral margin of the upper jaw; rostral tip of the maxilla slopes continuously; a depression present on the dorsal snout behind the naris; 25 dentary teeth. Based on our observations of CXM-LT9401, the lacrimal orbital margin has a slight rostrodorsal slope, the premaxillary process of the maxilla does not slope continuously, a depression on the dorsal snout behind the naris is also

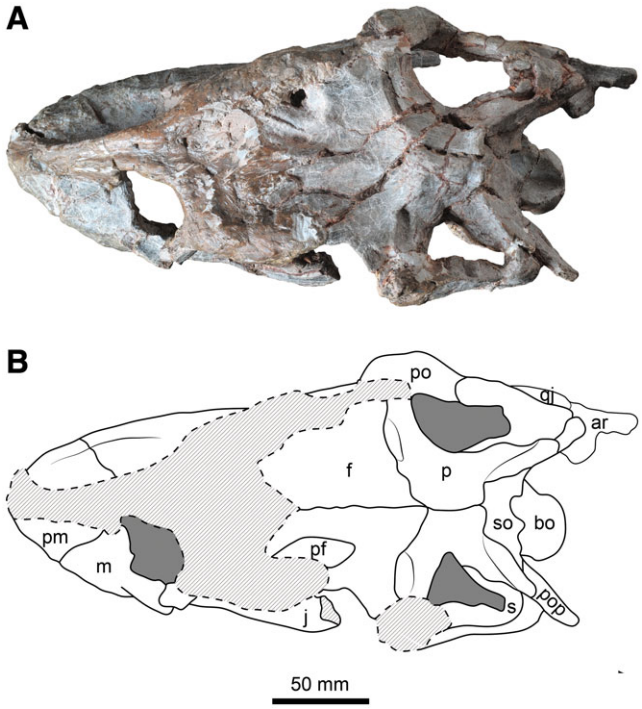

Fig. 4. Photograph **(A)** and interpretative line drawing **(B)** of the cranium of LFGT-ZLJ0113 in dorsal view. Dark gray fills represent openings, diagonal lines represent missing parts, and dashed lines represent fracture.

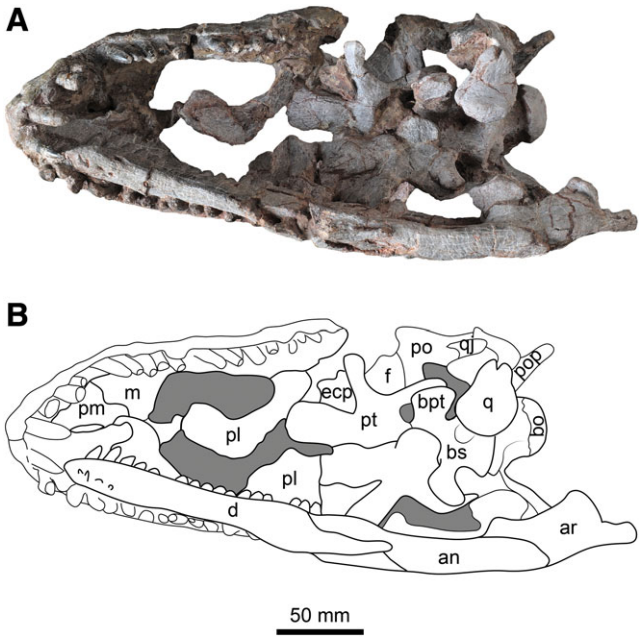

Fig. 5. Photograph **(A)** and interpretative line drawing **(B)** of the cranium of LFGT-ZLJ0113 in ventral view. (Dark gray fills represent openings.)

present in many other basal sauropodomorphs, such as *Lufengosaurus* (Barrett et al. 2005), and the number of dentary teeth cannot be reliably ascertained. However, the inflection at the base of the dorsal premaxillary process could be considered a distinguishing feature of CXM-LT9401 as noticed by Lü et al. (2010), and is only present in *Melanorosaurus* (NMQR 3314) (Yates 2007). Unfortunately, the corresponding feature is not preserved in LFGT-ZLJ0113. Our cladistic analysis recovers LFGT-ZLJ0113 and CXM-LT9401 in a sister group (see later). Considering that the two specimens come from the same horizon and the sites where they were discovered are relatively close to one another (about 7 km apart; Fig. 1), *C. lufengensis* is here proposed to be a junior synonym of *J. xinwaensis* and CXM-LT9401 is referred to *J. xinwaensis.*

DESCRIPTION

The description is focused on the holotype (LFGT-ZLJ0113), supplemented with information from CXM-LT9401. Measurements of LFGT-ZLJ0113 are given in the Supporting Information Table S6. Lü et al. (2010) had given a general description and measurement of CXM-LT9401, so those of the specimen are not necessary to be repeated, and only the required changes are proposed here.

General Features

The skull of LFGT-ZLJ0113 is three-dimensionally preserved, but it has undergone some torsion resulting in the misalignment of its right and left sides. Further, the rostral region of the skull roof has been crushed dorsoventrally such that the nasal processes of the premaxillae, the ascending process of the right maxilla, dorsal parts of the lacrimals, the nasals, and the prefrontals are all damaged (Figs. 2–4). Additionally, the right mandibular ramus is shifted medially to the upper jaw and the dentary tooth-bearing is obscured as a consequence, whereas the left one is isolated and nearly complete (Fig. 7). Several regions of the palate and the braincase are also fragmented or obscured by matrix and many small cracks are present on bone surfaces.

In lateral view, the skull of LFGT-ZLJ0113 is long and wedge-shaped in outline (Figs. 2–3). It is about twice as long (as measured from the tip of the premaxilla to the caudal margin of the quadrate) as it is high (as measured from the dorsal margin of the parietal to the ventral margin of the quadrate). The skull of CXM-LT9401 has a similar length-to-height ratio according to the original measurements (Lü et al. 2010, table 1). In dorsal view, the skull of LFGT-ZLJ0113 is subtriangular, and tapers gradually from its widest point across the postorbital to the tip of the snout (Fig. 4). The occiput of the skull is subrectangular in caudal view, and the occipital plate is slightly inclined rostrodorsally (Fig. 6).

The cranial openings of LFGT-ZLJ0113 are relatively large. The shape of the external naris is deduced to be subtriangular although its rostrodorsal border cannot be defined (Fig. 2). The caudal-most tip of this opening is located caudal to the level of the rostral margin of the antorbital fenestra (Fig. 2) and the caudal margin of the external naris of CXM-LT9401 (Fig. 8). This is contrary to the condition of the antorbital fenestra in other basal sauropodomorphs. This feature is thus considered autapomorphic for *Jingshanosaurus.* Additionally, the external naris of the CXM-LT9401 is large, with a maximum diameter equivalent to 24% of the total skull

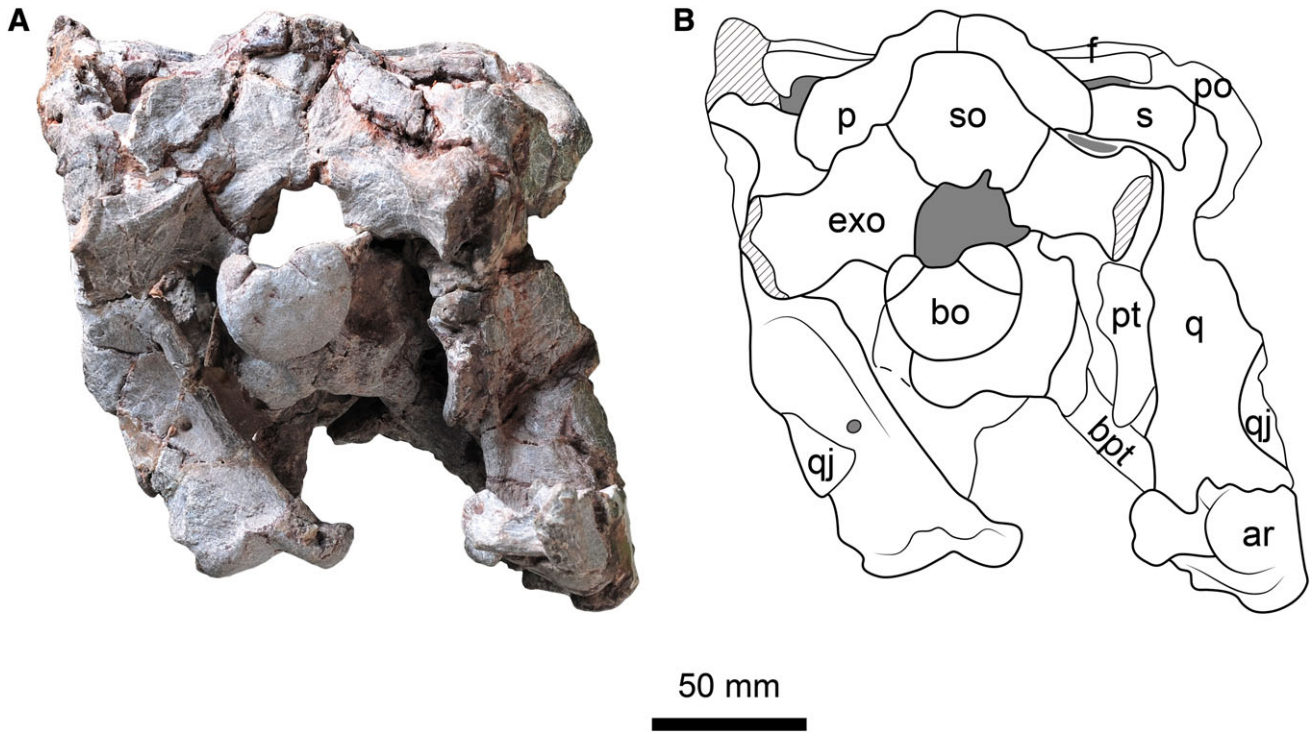

Fig. 6. Photograph **(A)** and interpretative line drawing **(B)** of the cranium of LFGT-ZLJ0113 in caudal view. Dark gray fills represent openings, diagonal lines represent missing parts, and dashed lines represent fracture.

length, but the majority of other basal sauropodomorphs (*Plateosaurus*, *Massospondylus*, *Riojasaurus*, *Mussaurus*, and *Coloradisaurus*) have relatively smaller external nares, with diameters that range from 14% to 18% of the total skull length, that of *Yunnanosaurus* is only 10% (Barrett et al. 2007). In lateral view, the antorbital fenestra of LFGT-ZLJ0113 is large, forms an approximately right triangle and sets within a broad, subtriangular antorbital fossa. The orbit is the largest opening in the skull, it has a subtriangular outline, and measures approximately a quarter of the total length of the skull (Fig. 3). Although the ventral process of the postorbital is broken, the ventral portion of the orbit is somewhat constricted (Fig. 3), the shape in life position should be the same as in CXM-LT9401 (Fig. 8). The shape

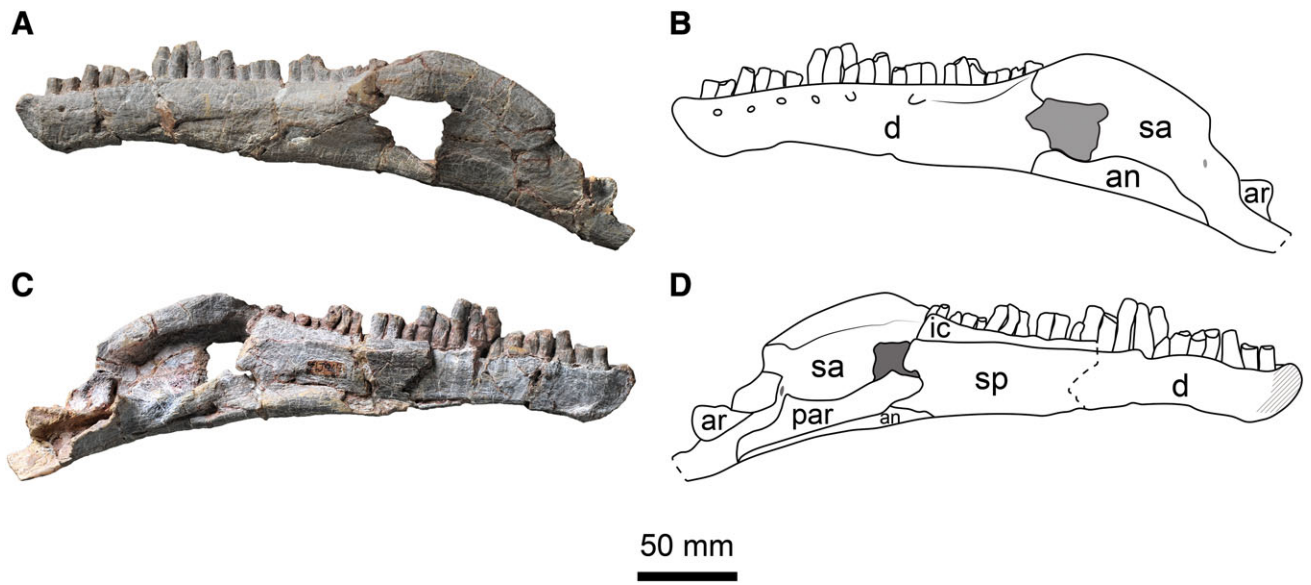

Fig. 7. Photographs and interpretative line drawings of the left mandibular ramus of LFGT-ZLJ0113 in lateral (**A, B**) and medial (**C, D**) views. Dark gray fills represent openings, and dashed lines represent fracture.

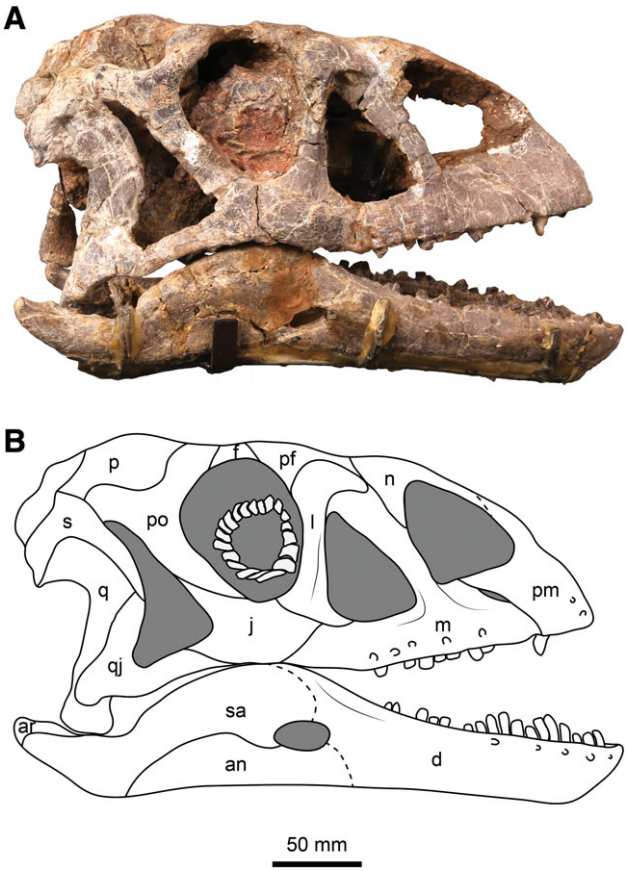

Fig. 8. Photograph **(A)** and interpretative line drawing **(B)** of CXM-LT9401 in right lateral view. Dark gray fills represent openings and dashed lines represent fracture. Note the skull looks like a little shorter than the lower jaw, and this visual difference is caused by mounting position and camera angle.

of the infratemporal fenestrae of LFGT-ZLJ0113 cannot be identified due to the fractured and missing bones in lateral views. In CXM-LT9401, the rostral margin of the infratemporal fenestra extends under the rear half of the orbit. The supratemporal fenestra of LFGT-ZLJ0113 is rostrocaudally elongated and subtriangular in dorsal view, with an obtuse, smooth medial border (Fig. 4). The long axis of the supratemporal fenestra of CXM-LT9401 is also longitudinally oriented (see Supporting Information Fig. S2A) and not transversely oriented as originally described (Lü et al. 2010).

Skull Roof

Premaxilla. The premaxilla of LFGT-ZLJ0113 preserves a robust, rostrocaudally short main body with a strip-shaped caudolateral process. The nasal process is broken. The nasal process of CXM-LT9401 is short and gracile in lateral and anterior view, as in other basal sauropodomorphs. In lateral view, the main body of the premaxilla in LFGT-ZLJ0113 is rectangular and bears four elongated premaxillary teeth (Figs. 2–3), similar to the condition in most basal sauropodomorphs. The lateral surface of the premaxilla is slightly convex, and at least two large nutrient foramina can be identified on the left side. The caudolateral process of the premaxilla extends caudally to overlap the rostrodorsal part of the premaxillary process of the maxilla, and gently reduces its height toward the distal end. In lateral view, a slot-shaped subnarial foramen is present at the middle of the premaxilla-maxilla suture (Fig. 3), as well as that of CXM-LT9401. It is worth noting that the premaxilla of CXM-LT9401 has an inflection at the base of its nasal process (Fig. 8), resembling the condition in *Melanorosaurus* (NMQR 3314), but this region of LFGT-ZLJ0113 is missing.

Maxilla. The maxilla of LFGT-ZLJ0113 consists of two major parts: a horizontally directed tooth-bearing ramus and a caudodorsally directed ascending process (the latter part of the right maxilla is missing). In lateral view, the main process of the maxilla is straight, and gradually tapers caudally. Almost five poorly preserved nutritive foramina are present on the lateral surface of the main ramus of the maxilla, and most of which are oriented caudoventrally (Fig. 3). The main ramus of the maxilla in CXM-LT9401 presents the same condition, and five similarly sized foramina are arranged linearly, and not irregularly as originally described (Lü et al. 2010). There is no vestige of a lateral maxillary ridge, differing from the condition in *Lufengosaurus* (Barrett et al. 2005) and *Melanorosaurus* (NMQR 3314) (Yates 2007). The height of the medial plate of the alveolar part of the maxilla is only slightly shorter than that of the lateral one, indicating that the "lateral plate" is absent, although it is present in *Yizhousaurus* (Zhang et al. 2018) and *Aardonyx* (Yates et al. 2010). The tooth row extends along nearly the entire length of the maxilla and contains 15–16 maxillary teeth (Fig. 5). The ascending process of the left maxilla is narrow in its mid-portion, and it forms most of the caudal margin of the external naris and the rostral margin of the antorbital fenestra. The caudoventral corner of the ascending process is excavated, giving rise to a "medial lamina" that comprises the rostroventral boundaries of the shallow antorbital fossa (Fig. 2), but this condition is absent in some sauropodomorphs (e.g., *Plateosaurus*, *Lufengosaurus*, *Anchisaurus*, and *Yunnanosaurus*). The dorsal part of the ascending process is broken. The ascending process widens dorsally in CXM-LT9401 (Fig. 8), but it is not as wide as that of *Lufengosaurus* or *Yizhousaurus*.

Lacrimal. The left lacrimal is more complete than the right one in LFGT-ZLJ0113. The lacrimal consists of a relatively robust main shaft and a short rostrodorsal process, which is obscured by plaster, giving the bone an inverted "L"-shape in lateral view. The main shaft is rostrodorsally oriented along its length about 80° relative to the ventral margin of the maxilla, as well as the condition in CXM-LT9401. It is much closer to vertical than the condition present in most basal sauropodomorphs, particularly other Lufeng taxa (e.g., *Lufengosaurus*, *Xingxiulong*, and *Yunnanosaurus*), but contrary to that in *Yizhousaurus* (Zhang et al. 2018), in which the lacrimal is vertical or even slightly caudodorsally oriented (Zhang et al. 2018). The ventral part of the main shaft is caudally expanded without a shallow fossa present in *Yunnanosaurus* (Barrett et al. 2007), and articulated with the rostrodorsal margin of the jugal ventrally. The rostroventral corner has a minor contribution to the caudal margin of the antorbital fossa (Fig. 3). Lü et al. (2010) indicated that the dorsal exposure of the lacrimal of CXM-LT9401 is absent, however, this

is not the case: in fact the lacrimal is exposed in dorsal view (see Supporting Information Fig. S2A).

Prefrontal. Only the caudal process of the left prefrontal in LFGT-ZLJ0113 is preserved, with a subtriangular outline in dorsal view (Fig. 4). This process has an extensive overlapping contact with the rostral part of the frontal. The prefrontal of CXM-LT9401 is shorter than the diameter of its orbit.

Frontal. The frontals of LFGT-ZLJ0113 are subtrapezoidal, transversely broad plates in dorsal view. They are sutured to one another by a low, straight midline ridge. The rostral end of the frontal is narrow without a midline boss which is autapomorphic for *Yunnanosaurus* (Barrett et al. 2007), and it may insert between the prefrontal and the nasal, although its boundary with the nasal cannot be determined accurately due to breakage (Fig. 4). Each frontal is caudally expanded and concave dorsally to form a parasagittal depression on its dorsal surface. The lateral margin of the frontal is emarginated to form most of the dorsal margin of the orbit, as in most basal sauropodomorphs (with the exception of *Plateosaurus* and *Lufengosaurus*). The caudal margin of the frontal is also concave, forming long curved contacts with the parietal caudally and the postorbital caudolaterally. The frontal is excluded from the margin of the supratemporal fenestra by the parietal and postorbital, but contributes to the supratemporal fossa, which is also common in other basal sauropodomorphs.

Parietal. The parietal of LFGT-ZLJ0113 is well preserved and consists of a robust main body with two laterally directed processes of subequal size, a rostrolateral process and a caudolateral process. The parietals are fused to one another, and no pineal foramen is present in dorsal view. The rostrolateral process is gently curved and extends laterally. This process contacts the frontal rostrally along a transversely curved suture and the rostrodorsal process of the postorbital laterally, together forming the rostral margin of the supratemporal fossa (Fig. 4). The dorsal surface of the rostrolateral process is gently concave along its length, and has no evidence of a prominent boss, which is one of the diagnostic features of *Lufengosaurus* (Barrett et al. 2005). The caudolateral process of the parietal contacts the squamosal caudally, diverging from the midline of the main body at an angle of approximately 45° in dorsal view. This process is broadly exposed in caudal view, contacts the dorsal margin of the exoccipital, and together defines a small post-temporal fenestra at the middle of their suture (Fig. 6).

Postorbital. Only the rostrodorsal and caudodorsal processes of the postorbitals in LFGT-ZLJ0113 are preserved. In lateral view, the rostrodorsal process of the postorbital is a strap-like element, a little longer and slenderer than the caudodorsal process (Fig. 3). In dorsal view, the rounded tip of this process contacts with the frontal and the rostrolateral process of the parietal medially. The caudodorsal process is short and situated lower than the dorsal margin of the rostrodorsal process. This process has an extensive overlapping contact with the squamosal medially, forming the dorsal margin of the infratemporal fenestra. The ventral process of the postorbital in CXM-LT9401 extends rostroventrally and its transverse width is less than the rostrocaudal width at the mid-shaft, but *Yizhousaurus* possesses a transversely wider postorbital ventral process (Zhang et al. 2018).

Jugal. Only the maxillary processes of the jugals are preserved in LFGT-ZLJ0113. The maxillary process is dorsoventrally deep and tapers rostrally between the lacrimal and the maxilla with a blunt end (Fig. 2). This process makes no contribution to the border of the antorbital fenestra. The jugal of CXM-LT9401 is well preserved. The suborbital portion of the jugal is rostrocaudally short and dorsoventrally deep (Fig. 8), similar to the shortened jugal plate in more derived sauropods, and contrary to the elongated bars found in all other basal sauropodomorphs. Note that its sutural contact with the maxilla is incorrectly reconstructed in the original paper (Lü et al. 2010).

Quadratojugal. Both quadratojugals of LFGT-ZLJ0113 are damaged and no more than the caudoventral corners are preserved. This region is composed of a heel-like plate which attaches to the lateral surface of the quadrate and tapers dorsally to a point to reach the ventral tip of the squamosal. However, the suture is not clear (Fig. 3). The caudoventral processes in both LFGT-ZLJ0113 and CXM-LT9401 are expanded, like those of most basal sauropodomorphs, but different with the less developed condition of *Yunnanosaurus* (Barrett et al. 2005).

Squamosal. The right squamosal of LFGT-ZLJ0113 appears to be complete while the left one is ventrally damaged. The squamosal is a tetraradiate bone that gives rise to rostral, ventral, caudoventral, and caudomedial processes. The rostral process is robust and largely overlapped by the postorbital laterally, and forms the lateral margin of the supratemporal fenestra. The ventral process is stout at the base, and tapers ventrally toward its contact with the quadratojugal along the rostrolateral surface of the shaft of the quadrate (Fig. 3). The length-to-width ratio of the ventral process is approximately 4, similar to the condition in CXM-LT9401, not approximately 2.8 as described by Lü et al. (2010). There is a recess between the ventral and the caudoventral processes that clasps the quadrate head. The caudoventral process is short and gently curved in lateral view. It contacts the paroccipital process caudoventrally. Finally, the caudomedial process of the squamosal is short and slender, contacting the caudolateral process of the parietal medially (Fig. 6).

Quadrate. Both quadrates of LFGT-ZLJ0113 are present, but have suffered some damage. The right quadrate is articulated with the ramus of the mandible with its ventral end covered by the glenoid in lateral view. The left quadrate is exposed ventrally. The quadrate consists of a robust shaft that divides into a rostrolateral quadratojugal wing and a rostromedial pterygoid wing, together forming a large concave area on its rostral surface. The rostrolateral wing of the quadrate contacts the ventral process of the squamosal dorsally and the ascending process of the quadratojugal ventrally (Fig. 3). The rostromedial wing forms a large plate and contacts with the pterygoid medially, and occupies more than 70% the length of the quadrate. The quadrate shaft is robust and slightly bowed rostrally. Its caudal surface appears to be deeply excavated and bears a conspicuous crest on the caudomedial margin in caudal view. The small and circular quadrate foramen can be seen on the

caudal surface (Fig. 6), and the quadrate foramen also presents in CXM-LT9401, although it is not so clear (see Supporting Information Fig. S2C in). The ventral articular surface of the quadrate is transversely expanded and divided into two condyles by a shallow sulcus, and the medial condyle is larger and extends more ventrally than the lateral one (Fig. 5).

Palatal Elements

Palatine. The palatines of LFGT-ZLJ0113 are not well preserved, especially the right one which only preserves part of the maxillary process. The left palatine has a small displacement, but its maxillary process is still articulated with the maxilla along its lateral margin (Fig. 5). This process extends medially to meet the pterygoid then expands rostrocaudally to merge with the main body of the pterygoid. The main body is a dorsoventrally expanded thin plate, with its caudal margin articulated with the pterygoid caudomedially (Fig. 3).

Pterygoid. The pterygoid of LFGT-ZLJ0113 is a complex element. The main body of the pterygoid is transversely wide in ventral view and gives rise to four distinct parts. The rostral palatine process tapers rostrally (the tip is broken), and contacts the palatine rostrally. The laterally projecting transverse flange of the pterygoid contacts the ectopterygoid rostrolaterally (Fig. 5). Caudally, the pterygoid has a transversely thin quadrate process and a short and stout median process, they diverge from one another at an angle of approximately 30°. A distinct socket for the basipterygoid process exists along the junction of the median process and the central part of the pterygoid (Fig. 5).

Ectopterygoid. Only fragments of the ectopterygoids are preserved in LFGT-ZLJ0113 (Fig. 3), which articulate with the ventral surface of the pterygoid.

Braincase

Supraoccipital. The occipital plate of LFGT-ZLJ0113 slightly inclines rostrodorsally. The supraoccipital has a roughly pentagonal outline, and is transversely slightly wider than dorsoventrally high, occupying the dorsal half of the occipital region of the skull (Fig. 6). The condition in CXM-LT9401 is the same, other than the higher than wide supraoccipital stated by Lü et al. (2010). The dorsal margin of the supraoccipital of LFGT-ZLJ0113 has a straight contact with the parietals, and the post-parietal fenestra is absent along their suture. The median ridge of the supraoccipital is low and rounded and extends along the dorsal half of the midline (Fig. 6). Its suture with the exoccipital-opisthotic complex is obscured. The ventral margin of the supraoccipital bears two small processes and forms the dorsal margin of the foramen magnum.

Exoccipital-opisthotic. The exoccipital-opisthotic of LFGT-ZLJ0113 is a robust and complex element. It contacts the supraoccipital dorsally, the basioccipital ventrally, and borders the foramen magnum laterally. The paroccipital process projects caudolaterally and ventrally, expanding distally to a blunt and thick end (Fig. 6).

Basioccipital. The basioccipital borders the foramen magnum ventrally. It contacts the exoccipital dorsolaterally and comprises the occipital condyle caudally. The occipital condyle is semilunar in outline and slightly convex (Fig. 6). It constricts to the short condylar neck rostrally and the ventral surface of the neck appears to be flat. Further rostrally, the basioccipital contributes to the basal tubera. The basal tuberae is a rostrocaudally compressed ridge composed of the basisphenoid and basioccipital at its junction, and this junction is not completely fused with one rostrolaterally opened notch on each side (Fig. 5).

Basisphenoid. The basisphenoid of LFGT-ZLJ0113 is well exposed in ventral view and constitutes the rostral region of the braincase floor. The rostroventral region of the basisphenoid is gently concave transversely, and a deep median fossa exists on the caudoventral surface between the basal tubera and the basipterygoid processes (Fig. 5). The basipterygoid processes are short, rod-like projections with a subelliptical cross section, and are ventrolaterally directed.

Parasphenoid. Only the rostral part of the parasphenoid rostrum is visible through the broken orbit in lateral view (Fig. 3). It appears to be subtriangular in lateral view and oriented rostrally and slightly dorsally with respect to the braincase floor, showing that the braincase floor is relatively bent, as in *Yizhousaurus* (Zhang et al. 2018) and *Melanorosaurus* (NMQR 3314) (Yates 2007), but not like the presence of the "stepped" braincase in most basal sauropodomorphs.

Mandible

Both mandibular rami of LFGT-ZLJ0113 are well preserved. The right one is in contact with the skull, and the majority of mandibular sutures are obscured. Although the external mandibular fenestra of the isolated left mandibular ramus is damaged (Fig. 7A,C), the outline of this fenestra is bounded rostrally by the dentary, caudodorsally by the surangular, and caudoventrally by the angular. It makes up roughly 10% of the total mandibular length. The undamaged, actual size of this fenestra should be smaller than 10%, contrary to the relatively large size in most basal sauropodomorphs, whereas *Riojasaurus* and *Yizhousaurus* possess a considerably smaller fenestra (5∼7% of the mandible length). In lateral view, the jaw articulation is below the level of the dentary tooth row, as in other basal sauropodomorphs, but the jaw joint of *Massospondylus* and *Yunnanosaurus* is on the same level as the dentary tooth row.

Dentary. The dentary of LFGT-ZLJ0113 is elongated and comprises over half of the total mandibular length. It maintains an almost constant depth along the rostral ramus, and increases slightly in depth caudally toward its contact with the post-dentary bones. The ratio of the height to length of the dentary is around 0.28, and CXM-LT9401 also has a relatively higher dentary. In this way, both specimens differ from most other basal sauropodomorphs, which have a lower dentary (ratio: <0.2). The lateral surface of the dentary in LFGT-ZLJ0113 is gently convex with a rounded, low, and longitudinal ridge extending one third of the length of the caudal dentary (Fig. 7A). This ridge indicates the existence of the buccal emargination, which is common in most basal sauropodomorphs. This ridge is also seen in CXM-LT9401 (Fig. 8), not absent as Lü et al. (2010)

described. The tooth row of LFGT-ZLJ0113 is relatively long and occupies most of the dorsal margin of the dentary. Several nutrient foramina are found just ventral to the alveolar margin on the lateral surface of the dentary. Based on preserved teeth and alveoli, the number of dentary teeth is estimated to be 22 in the left and 20 in the right. Although the dentary teeth of CXM-LT9401 cannot be accurately determined, its number of teeth does not differ substantially from that of LFGT-ZLJ0113. In medial view, the symphysis is small and subelliptical in outline (Fig. 7C).

Surangular. The surangular of LFGT-ZLJ0113 is an elongated and relatively large element constituting most of the caudodorsal region of the mandibular ramus. The lateral surface of the surangular is slightly convex. It borders much of the caudodorsal margin of the external mandibular fenestra. Its dorsal margin is medially inflected to form the coronoid eminence, and then decreases in height caudally to approach the jaw articulation (Fig. 7A). The surangular covers the caudal end of the dentary rostrally, the lateral surface of the articular caudally, and the angular ventrally. The medial surface of the surangular is slightly concave, and a small foramen is present caudal to the coronoid eminence (Fig. 7D).

Angular. The angular of LFGT-ZLJ0113 is a large and strap-like element that wraps around the ventral region of the caudal portion of the mandibular ramus. In lateral view, it has a broad contact with the surangular dorsally and articulates with the dentary rostrally. Medially, it meets the prearticular along an almost straight suture dorsally (Fig. 7C).

Intercoronoid. The intercoronoid of LFGT-ZLJ0113 is a rostrocaudally elongated, dorsoventrally narrow, thin plate that covers the medial surface of the caudal half of the alveolar margin. The rostral part of the intercoronoid is broken (Fig. 7C).

Splenial. The caudal part of the splenial in LFGT-ZLJ0113 is preserved on the medial surface of the left mandible. It is a flat, sheet-like element that covers the dentary medially (Fig. 7C). No splenial foramen is visible due to the rostral damage to this bone.

Prearticular. The prearticular of LFGT-ZLJ0113 is rostrocaudally elongated and exposed in medial view. The ventral margin of the prearticular is conjoined with the angular along its entire length, and its caudal end contacts the ventromedial surface of the articular (Fig. 7C).

Articular. The articular of LFGT-ZLJ0113 is an irregular, block-like element that lies dorsal to the prearticular and contacts the surangular laterally. Caudal to the glenoid is a stout process that projects medially, which is also noted to be present in CXM-LT9401 (Lü et al. 2010). The retroarticular process of LFGT-ZLJ0113 has a blunt tip, and its rostrocaudal length is greater than the depth of the mandibular ramus below the glenoid, a feature also present in *Coloradisaurus* (Apaldetti et al. 2014) and *Lufengosaurus* (Barrett et al. 2005).

Dentition

Most of the teeth are preserved in both the upper and lower jaws of LFGT-ZLJ0113. However, many of them are broken apically with the mesiodistal margins obscured. All the teeth are long, lanceolate, and labiolingually compressed. The four premaxillary teeth are the longest teeth apicobasally. The premaxillary tooth crowns are asymmetrical and gently curve caudally (Fig. 3). The maxillary tooth crowns are mesiodistally expanded slightly relative to the roots, but this is not as pronounced as in other basal sauropodomorphs. The labial surfaces of the tooth crowns are slightly convex, whereas the lingual surfaces are almost flat. The tooth enamel on the labial surfaces are smooth and display gracile longitudinal striations. No wear facets are present (see Supporting Information Fig. S1B). The dentary teeth are closely packed, similar to the condition of the maxillary teeth. The serrations are poorly preserved but present in maxillary and dentary teeth, and they are restricted to the apical region of the crowns. Although the premaxillary teeth of CXM-LT9401 are broken, but the morphology of the maxillary and dentary teeth is almost the same as those of LFGT-ZLJ0113, with distally recurved tooth crowns, finely wrinkled tooth enamel and mesiodistal tooth serrations.

DISCUSSION

Our phylogenetic analysis generated two most parsimonious trees (MPTs) with the following scores: tree length = 1,292 steps, consistency index (CI) = 0.333, and retention index (RI) = 0.690. The strict consensus tree is relatively well-resolved (Fig. 9). LFGT-ZLJ0113 is recovered as a sister taxon of CXM-LT9401, which supports the assignment of CXM-LT9401 to *J. xinwaensis*. This clade (=*J. xinwaensis*) is supported by four synapomorphies: level of the caudal margin of external naris is caudal to the mid-length of the maxillary tooth row and the rostral margin of the antorbital fenestra (character.state: 19.2); height-to-length ratio of the dentary is greater than 0.2 (character.state: 98.1); length of the retroarticular process is greater than the depth of the mandible below the glenoid (character.state: 105.1); and the tooth crowns have a distally recurved long axis (character.state: 116.0). The cranium of CXM-LT9401 is better preserved than that of LFGT-ZLJ0113 and has additional features that can also be considered diagnostic for *J. xinwaensis*. These include the inflection at the base of the dorsal premaxillary process, the slightly rostrodorsally inclined lacrimal, the ventrally constricted subtriangular orbit, and the rostrocaudally shortened jugal at the suborbital region.

Jingshanosaurus was recovered as the second diverging clade of Sauropodiformes between *Xingxiulong* and *Yunnanosaurus*, and they together represent the basalmost lineages of this clade. However, the cranial morphology of these three taxa demonstrate clear differences. Contrary to *Jingshanosaurus*, in *Xingxiulong*, the lacrimal shaft inclines rostrodorsally, the orbital is subcircular with a slender jugal bordering its ventral margin, the rostroventral corner of the infratemporal fenestra does not extend below the orbit, the diverging angle between the jugal and the quadratojugal is close to 90°, and the surangular and angular extend rostrally to the relatively large external mandibular fenestra (Wang et al. 2017). These features indicate that *Xingxiulong* probably had a relatively long and low cranial profile

Fig. 9. Strict consensus of phylogenetic analysis depicting the position of *J. xinwaensis.* Dark dot represents node-based definitions, and arrows represent stem-based definitions; numbers below the nodes represent bootstrap frequencies higher than 50% (left) and Bremer support values higher than 1 (right); the two specimens of *Jingshanosaurus* are colored in orange, and other material from Lufeng are colored in green. Abbreviations: CI, consistency index; MPTs, most parsimonious trees; RI, retention index.

compared to *Lufengosaurus*, a member of Massospondylidae also from the Lower Jurassic of Lufeng, and *Plateosaurus*, a more basal sauropodomorph diverging prior to Sauropodiformes and Massospondylidae (Fig. 9). *Yunnanosaurus* also has a low and elongated skull with its skull length more than twice its height. *Yunnanosaurus* possesses many unique features that are absent not only in *Jingshanosaurus* but also in all known basal sauropodomorphs, such as an extremely small external naris (less than 10% of maximum skull length), a lack of nutritive foramina on the lateral surface of maxilla, and a lack of denticles on the maxillary teeth (Barrett et al. 2007).

As a basal sauropodiform, *Jingshanosaurus* is distinguished from its close relatives and possesses many unique cranial features including: (1) a relatively high skull about half of its length; (2) a moderately developed external narial fossa about the same size as the orbit as evidenced by the elongated external naris extending

caudal to the mid-length of the maxillary tooth row and the rostral margin of the antorbital fenestra; (3) a relatively robust lower jaw suggested by the heightened dentary with its height-to-length ratio greater than 0.2 and a reduced external mandibular fenestra less than 10% of the total mandibular length; (4) relatively primitive dentition with elongated and serrated teeth with recurved mesial tooth crowns. These characters represent a mosaic of both derived and primitive features in the cranium of *Jingshanosaurus* likely due to the basal nature of *Jingshanosaurus.* However, controversies still exist regarding the phylogenetic placement of many of these taxa. For example, a cranial-only cladistic analysis recovers *Yunnanosaurus* as more basal than both *Xingxiulong* and *Jingshanosaurus*, and even *Lufengosaurus* and *Plateosaurus* (Zhang et al. 2018).

Jingshanosaurus has been known for over 20 years, but in spite of its importance and remarkable preservation, its cranial osteology had not been studied since it was originally described. We hope this study will provide a basis for future studies to allow for a better understanding this important dinosaur. More studies on not only *Jingshanosaurus,* but other Lufeng taxa will allow for better reconstructions of the ecomorphotypic diversity of the Lower Jurassic Lufeng and potentially help to decipher the origin and early evolution of sauropodiforms.

ACKNOWLEDGEMENTS

The authors thank the Lufeng World Dinosaur Valley Museum staff for preparing the cranium of LFGT-ZLJ0113 and Guo-Fu Wang for access to the material of CXM-9401. We are grateful to Peter Dodson and Brandon Hedrick for inviting us to contribute to this special issue. We also thank Xiao-Chun Wu for valuable discussion, as well as the editor and two anonymous reviewers for constructive criticism that improved this manuscript. We are appreciative of Wei Gao for taking the photographs in Figures 2–7, and many thanks to other staff at Institute of Vertebrate Paleontology and Paleoanthropology, Chinese Academy of Sciences for support.

LITERATURE CITED

Apaldetti C, Martinez RN, Alcober OA, Pol D. 2011. A new basal sauropodomorph (Dinosauria: Saurischia) from Quebrada del Barro Formation (Marayes-El Carrizal Basin), Northwestern Argentina. PLoS ONE 6:e26964.

Apaldetti C, Martinez RN, Pol D, Souter T. 2014. Redescription of the Skull of *Coloradisaurus brevis* (Dinosauria, Sauropodomorpha) from the Late Triassic Los Colorados Formation of the Ischigualasto-Villa Union Basin, northwestern Argentina. Journal of Vertebrate Paleontology 34(5):1113–1132.

Apaldetti C, Pol D, Yates A. 2013. The postcranial anatomy of *Coloradisaurus brevis* (Dinosauria: Sauropodomorpha) from the Late Triassic of Argentina and its phylogenetic implications. Palaeontology 56:277–301.

Barrett PM, Upchurch P, Wang X-L. 2005. Cranial osteology of *Lufengosaurus huenei* Young, 1941 (Dinosauria : Prosauropoda) from the Lower Jurassic of Yunnan, People's Republic of China. J Vertebr Paleontol 25(4):806–822.

Barrett PM, Upchurch P, Zhou X-D, Wang X-L. 2007. The skull of *Yunnanosaurus huangi* Young, 1942 (Dinosauria: Prosauropoda) from the Lower Lufeng Formation (Lower Jurassic) of Yunnan, China. Zool J Linn Soc 150(2):319–341.

Chapelle KEJ, Choiniere JN. 2018. A revised cranial description of *Massospondylus carinatus* Owen (Dinosauria: Sauropodomorpha) based on computed tomographic scans and a review of cranial characters for basal Sauropodomorpha. PeerJ 6:e4224.

Cooper MR. 1981. The prosauropod dinosaur *Massospondylus carinatus* Owen from Zimbabwe: its biology, mode of life and phylogenetic significance. Occas Pap Natl Mus Monu Rhodesia Ser B 6: 689–840.

Ezcurra MD. 2010. A new early dinosaur (Saurischia: Sauropodomorpha) from the Late Triassic of Argentina: a reassessment of dinosaur origin and phylogeny. J Syst Palaeontol 8(3):371–425.

Galton PM. 1990. Basal Sauropodomorpha-Prosauropoda. In: Weishampel DB, Dodson P, Osmólska H, editors. *The Dinosauria*. Berkeley: University of California Press. p 320–344.

Galton PM, Cluver MA. 1976. *Anchisaurus capensis* (Broom) and a revision of the Anchisauridae (Reptilia, Saurischia). Ann S Afr Mus 69:121–159.

Galton PM, Upchurch P. 2004. Prosauropoda. In: Weishampel DB, Dodson P, Osmólska H, editors. *The Dinosauria*. 2nd ed. Berkeley: University of California Press. p 232–258.

Lü J-C, Kobayashi Y, Li T-G, Zhong S-M. 2010. A new basal sauropod dinosaur from the Lufeng Basin, Yunnan Province, southwestern China. Acta Geol Sin-Engl Ed 84(6):1336–1342.

Martínez RN. 2009. *Adeopapposaurus mognai*, gen. et sp. nov. (Dinosauria: Sauropodomorpha), with comments on adaptations of basal Sauropodomorpha. J Vertebr Paleontol 29:142–164.

McPhee BW, Bonnan MF, Yates AM, Neveling J, Choiniere JN. 2015. A new basal sauropod from the pre-Toarcian Jurassic of South Africa: evidence of niche-partitioning at the sauropodomorph–sauropod boundary? Sci Rep 5:13224.

McPhee BW, Choiniere JN. 2017. The osteology of *Pulanesaura eocollum*: implications for the inclusivity of Sauropoda (Dinosauria). Zool J Linn Soc 182:830–861.

Otero A, Krupandan E, Pol D, Chinsamy A, Choiniere J. 2015. A new basal sauropodiform from South Africa and the phylogenetic relationships of basal sauropodomorphs. Zool J Linn Soc 174:589–634.

Otero A, Pol D. 2013. Postcranial anatomy and phylogenetic relationships of *Mussaurus patagonicus* (Dinosauria, Sauropodomorpha). J Vertebr Paleontol 33:1138–1168.

Sekiya T. 2010. A new prosauropod dinosaur from Lower Jurassic in Lufeng of Yunnan. Global Geology 29(1):6–15.

Sekiya T, Dong Z-M. 2010. A new juvenile specimen of *Lufengosaurus huenei* Young, 1941 (Dinosauria: Prosauropoda) from the Lower Jurassic Lower Lufeng Formation of Yunnan, southwest China. Acta Geologica Sinica - English Edition 84(1):11–21.

Sereno PC. 1999. The evolution of dinosaurs. Science 284:2137–2147.

Smith ND, Pol D. 2007. Anatomy of a basal sauropodomorph dinosaur from the Early Jurassic Hanson Formation of Antarctica. Acta Palaeontol Pol 52:657–674.

Upchurch P, Barrett PM, Galton PM. 2007. A phylogenetic analysis of basal sauropodomorph relationships: Implications for the origin of sauropod dinosaurs. Spec Pap Palaeontol 77:57–90.

Wang G. 2004. The *Jinshanosaurus* discovered at Tanghai. Lufeng Yunnan Geol 23:77–82. in Chinese.

Wang Y-M, You H-L, Wang T. 2017. A new basal sauropodiform dinosaur from the Lower Jurassic of Yunnan Province, China. Sci Rep 7:41881. https://doi.org/10.1038/srep41881.

Yates AM. 2004. *Anchisaurus polyzelus* (Hitchcock): the smallest known sauropod dinosaur and the evolution of gigantism among sauropodomorph dinosaurs. Denver Post 230:1–58.

Yates AM. 2007. The first complete skull of the Triassic dinosaur *Melanorosaurus* Haughton (Sauropodomorpha: Anchisauria). In: Barrett PM, Batten DJ, editors. *Evolution and Palaeobiology of Early Sauropodomorph Dinosaurs*. London: Palaeontological Association. p 9–55.

Yates AM, Bonnan MF, Neveling J, Chinsamy A, Blackbeard MG. 2010. A new transitional sauropodomorph dinosaur from the Early Jurassic of South Africa and the evolution of sauropod feeding and quadrupedalism. Proc Royal Soc B: Biolog Sci 277:787–794.

Young C-C. 1941a. A complete osteology of *Lufengosaurus hueni* Young (gen. et sp. nov.) from Lufeng, Yunnan, China. Palaeontologica Sinica New Series C 7:1–53.

Young C-C. 1941b. *Gyposaurus sinensis* Young. (sp. nov.), a new Prosauropoda from the Upper Triassic beds at Lufeng, Yunnan. Bull Geolog Soc China 21:205–253.

Young C-C. 1942. *Yunnanosaurus huangi* Young (gen. et sp. nov.), a new Prosauropoda from the Red Beds at Lufeng. Yunnan Bull Geolog Soc China 22(1–2):63–104.

Young C-C. 1947. On *Lufengosaurus magnus* Young (sp. nov.) and additional finds of *Lufengosaurus huenei* Young. Palaeontologica Sinica New Series C 12:1–53.

Young C-C. 1951. The Lufeng saurischian fauna in China. Palaeontologia Sinica, New Series C 13:1–94.

Zhang Q-N, You H-L, Wang T, Chatterjee S. 2018. A new sauropodiform dinosaur with a 'sauropodan' skull from the Lower Jurassic Lufeng Formation of Yunnan Province, China. Sci Rep 8:13464. https://doi.org/10.1038/s41598-018-31874-9.

Zhang Y-H, Yang Z-L. 1995. *A new complete osteology of Prosauropoda in Lufeng Basin Yunnan, China: Jingshanosaurus*. Kunming: Yunnan Publishing House of Science and Technology (in Chinese).